IET Nanobiotechnology

*Research Article*

IET Journals
The Institution of Engineering and Technology

# Iron oxide/gold nanoparticles-decorated reduced graphene oxide nanohybrid as the thermo-radiotherapy agent

ISSN 1751-8741
Received on 14th March 2020
Revised 15th April 2020
Accepted on 24th April 2020
E-First on 5th June 2020
doi: 10.1049/iet-nbt.2020.0106
www.ietdl.org

*Kave Moloudi[1], Hadi Samadian[2], Mehdi Jaymand[2], Ehsan Khodamoradi[1] ✉, Mojtaba Hoseini-Ghahfarokhi[1], Farshid Fathi[3]*

[1]*Department of Radiology and Nuclear Medicine, Alley School of Medicine, Kermanshah University of Medical Sciences, Kermanshah, Iran*
[2]*Nano Drug Delivery Research Center, Health Technology Institute, Kermanshah University of Medical Sciences, Kermanshah, Iran*
[3]*Department of Immunology, School of Medicine, Isfahan University of Medical Sciences, Isfahan, Iran*
✉ *E-mail: eh_medph@yahoo.com*

**Abstract:** The main focus of the current study is the fabrication of a multifunctional nanohybrid based on graphene oxide (GO)/iron oxide/gold nanoparticles (NPs) as the combinatorial cancer treatment agent. Gold and iron oxide NPs formed on the GONPs via the in situ synthesis approach. The characterisations showed that gold and iron oxide NPs formed onto the GO. Cell toxicity assessment revealed that the fabricated nanohybrid exhibited negligible toxicity against MCF-7 cells in low doses (<50 ppm). Temperature measurement showed a time and dose-dependent heat elevation under the interaction of the nanohybrid with the radio frequency (RF) wave. The highest temperature was recorded using 200 ppm concentration nanohybrid during 40 min exposure. The combinatorial treatments demonstrated that the maximum cell death (average of 53%) was induced with the combination of the nanohybrid with RF waves and radiotherapy (RT). The mechanistic study using the flow cytometry technique illustrated that early apoptosis was the main underlying cell death. Moreover, the dose enhancement factor of 1.63 and 2.63 were obtained from RT and RF, respectively. To sum up, the authors' findings indicated that the prepared nanohybrid could be considered as multifunctional and combinatorial cancer therapy agents.

## 1 Introduction

Breast cancer is the most frequent cancer among women and according to the last World Health Organisation reports, impacting 2.1 million women each year, which is ∼15% of all cancer deaths among women [1]. Conventional treatments for breast cancer include surgery, radiotherapy (RT), and chemotherapy. However, new methods such as hyperthermia, hormone therapy, target therapy with a radionuclide, gene therapy, and immunotherapy are under assessment in clinical trials [2]. Some reports showed that the recurrence rate of breast cancer 10-year after treatment is 4–18%. The treatment of recurrent local tumours by the conventional methods is not simple, so heavy chemotherapy and mastectomy are optional choices for out root tumours, and the consequences are awful.

Moreover, with the conventional treatment modalities such as the combination of radio-chemotherapy with and without surgery, maximum survival after recurrence is about 5 years [3]. According to the Dutch national guidelines, the standard treatment for loco-regionally recurrent breast cancer in a previously irradiated area is re-irradiation to a relatively low dose combined with hyperthermia. Hyperthermia is the artificially elevating the tissue temperature (range 40–44°C for 30–60 min), which adjuvant the other conventional treatment modalities to improve the treatment efficacy. This concept is based on the fact that hyperthermia enhances the blood circulation both around and within tumours. Furthermore, the cancer cells are more sensitive than healthy cells to elevated temperature [2, 4–6]. The application of hyperthermia shortly before or after RT improves the RT efficacy through the influencing intratumoural hypoxia and by inhibiting sublethal DNA damages repair in the tumour tissue. Moreover, the combination of hyperthermia with radiation reduces the total dose of radiation needed compared to RT alone, in which a higher dose is needed to achieve the same effect [7, 8].

Various methods have been developed to elevate the temperature of the tissues, such as alternative magnetic fields, lasers, ultrasound, and radio frequency (RF) waves. Amongst them, RF is an attractive approach that provides deep tissue penetration. The application of RF in the form of RF ablation is a currently established cancer treatment method for some cancers. It is reported that 13.56 MHz RF increased the temperature at the level of 40–46°C and was used to treat subcutaneous liver and pancreatic cancers in mice [9]. Despite these beneficial features, RF ablation suffers from some drawbacks, for instance invasive needle placement requirement, image-guidance, operator dependence, and collateral healthy tissue damages [10].

An alternative option over the conventional RF hyperthermia is the combination of RF wave with the heat converting agents. The application of some nanomaterials such as gold nanoparticles (AuNPs), carbon-based, and Si in combination with RF demonstrated significant results [11]. Nanomaterials provide additional opportunities to improve the efficacy of the current diagnostic and treatment modalities [12–15]. They have enhanced physicochemical properties and offer high specific surface areas favourable for the conjugation of various targeting and therapeutic agents [16]. It is demonstrated that some NPs, such as AuNPs can convert RF waves to heat and dissipate the generated heat to the surrounding tissue. NPs can penetrate into tumour tissue and effectively interact with cancer cells and dissipate the heat at the site of action. This approach reduces the time of exposure and increases the efficiency of RF-based therapy with fewer side effects [17–21].

Theranostics is an emerging concept for cancer detection and therapy. Theranostics agents provide diagnosis and treatment simultaneously. Iron oxide (IO) NPs (IONPs) are extensively used as magnetic resonance imaging (MRI) contrast agents. IONPs can be combined with other structures such as carbon-based nanomaterials to produce a theranostic agent [9, 22–25]. Graphene-based structures have found significant potential applications in biomedicine due to their fascinating properties [26–29]. Moreover, it is reported that graphene-based nanostructures can be considered as the support/template for different NPs formation. Accordingly, in the present study, we have introduced IONPs/AuNPs decorated reduced graphene oxide (rGO@IONPs@AuNPs) as a new complex to enhance and sensitise RF and RT effects.

## 2 Materials and methods

### 2.1 Chemicals

Graphite powder, Iron(II) chloride tetrahydrate ($FeCl_2{\cdot}4H_2O$), and Au(III) chloride trihydrate ($HAuCl_4{\cdot}3H_2O$) were purchased from Sigma-Aldrich, USA. Sulphuric acid, phosphoric acid, potassium permanganate, hydrogen peroxide, and hydrochloric acid were obtained from Merck, Darmstadt, Germany. 3-(4,5-Dimethylthiazol-2-yl)-2,5-diphenyltetrazolium bromide (MTT) and dimethyl sulphoxide were purchased from Carl Roth, Germany. Dulbecco's modified eagle medium, foetal bovine serum (FBS), penicillin–streptomycin (Pen–Strep), and Trypsin–Ethylenediaminetetraacetic acid (EDTA) were purchased from Gibco, Germany. MCF-7 cells were obtained from Pasteur Institute, Iran.

### 2.2 Fe–Au–GO nanocomplex synthesis

The modified Hummer's method was used to synthesis GO from pure graphite powder [30]. Briefly, 0.225 g of graphite powder was added to a mixture solution of sulphuric acid (27 ml) and phosphoric acid (3 ml) (volume ratio 9:1) under stirring condition. Then, 1.32 g of potassium permanganate was added to the prepared solution and stirred for 6 h until the solution became dark green. 0.675 ml of hydrogen peroxide was dropwise added to the solution and stirred for 19 min to remove the excess of potassium permanganate. In the next step, a mixture of hydrochloric acid (10 ml) and deionised water (DIW) (30 ml) was added and the solution centrifuged at 5000 rpm for 7 min at room temperature.

A modified hydrothermal approach was applied for Fe/AuNPs-decorated GO synthesis based on previous papers [31, 32]. Briefly, $FeCl_2{\cdot}4H_2O$ (199 mg) was dissolved in DIW (1.3 ml) under vigorous stirring for 30 min. The obtained solution was added to the previously prepared GO suspension under vigorous stirring for 2 h and sonicated for 30 s. In the next step, 1% $HAuCl_4{\cdot}3H_2O$ in DIW was added to the previous suspension, sealed in Teflon-lined stainless steel, and autoclaved at 200°C for 8 h. The resulted suspension was cooled down, washed with DIW several times, and finally, dried in an oven at 80°C for 3 h.

### 2.3 Fe–Au–GO nanocomplex characterisation

The synthesised Fe/AuNPs-decorated GO nanoplatform was characterised via transmission electron microscopy (TEM), scanning electron microscopy (SEM), dynamic light scattering (DLS), and zetasizer. For TEM imaging, a droplet (5 µl) of the diluted suspension was placed onto a carbon-coated copper grid and air-dried before observation via a Philips CM-100 microscope operating at 60 kV. The DLS and zeta potential measurements were conducted by zetasizer (Malvern Panalytical) on 1 ml of diluted suspension.

### 2.4 Fe–Au–GO nanocomplex toxicity assessment

The toxicity of the synthesised nanoplatform was measured using the MTT assay kit on MCF-7 cells. A number of $1 \times 10^4$ cells suspended in 100 µl DMEM cell culture medium supplemented with 10% FBS and 1% Pen–Strep were seeded in 96 well tissue culture plates and incubated for 24 h in laboratory condition (incubator 5% $CO_2$ and 95% $O_2$ at 37° C). Then, the seeded cells were treated with five different concentrations (10, 25, 50, 75, 100, and 200 ppm) of the NPs for another 24 h period. In this experiment, the control was the cells cultured on tissue culture plastic without treatment. After the incubation period, the MTT assay was performed according to the protocol of the MTT assay kit to measure the possible toxicity.

### 2.5 Thermal response evaluation

The thermal response of nanosuspensions under interaction with RF field with the power of 3 W/cm$^2$ and 900 MHz was assessed via the thermal recording approach. The stimulation was performed by a global system for mobile communication mobile phone simulator [33]. Three different concentrations of the nanoplatforms (50, 100, and 200 ppm) were subjected to RF radiation for 40 min and the thermal changes were recorded via a digital thermometer (APPA51) with a sensitivity of 0.10°C. The thermal changes of DIW were recorded as the control.

### 2.6 Cell death-induced by RF and RT treatments

A number of $2 \times 10^4$ cells were seeded in each well of the 96-wells plate, incubated for 24 h, and then divided into seven test groups (nanocomplex alone, RF alone, RT alone, nanocomplex + RF, nanocomplex + RT, and nanocomplex + RF + RT) and the control group (untreated cells). The RT therapy was performed with 6 MeV energy using an Elekta RT Precision radiation medicine to deliver 4 Gy dose at 500 CGy/min dose rate. The exposure was conducted at source object distance (SSD = 98 cm) and field of view (FOV = 15 × 15 cm). The cells were incubated in the laboratory incubator situation for 24 h after the exposure and the viability was measured by MTT assay kit. All the treatments were triplicated.

### 2.7 Apoptosis-induced by RF and RT treatments

The flow cytometry technique was utilised to evaluate the apoptosis elicited by the treatments. A number of $1 \times 10^6$ cells were seeded in each well of six-well-plate tissue culture plate and incubated for 24 h. The treatments were conducted based on the previously mentioned protocol. After the treatment, the cells were trypsinised, harvested, centrifuged, and washed twice with phosphate-buffered saline (PBS). The obtained cells were re-suspended in 400 µl PBS solution and 100 µl of the incubation buffer containing 2 µl of Annexin V (1 mg/ml) and 2 µl of propidium iodide (1 mg/ml) was added to the cell suspension.

### 2.8 Statistical analysis

The one-way analysis of variance followed by Tukey's test as the post-hoc analysis were applied using SPSS version 16 for the statistical analysis and the comparison of groups. All tests were performed in triplicate and the results were presented as mean values ± standard deviation (SD) with $P < 0.05$ as the statistical significance.

## 3 Results and discussion

### 3.1 Fe–Au–GO nanocomplex characterisation results

GO is a fascinating nanostructure with extraordinary physicochemical properties, which was used in the present study as the platform to support Fe and AuNPs formation. The combination of GO, Fe, and AuNPs provides a multifunctional nanoplatform applicable for cancer detection and therapy. The synthesised nanocomplexes were characterised via DLS, zetasizer, SEM, and TEM methods. The results of DLS showed that the prepared nanocomplex has an average size of 983 nm with the polydispersity index of 0.401. The zeta potential measurement illustrated that the nanocomplex has the zeta potential of −27.5 mV. However, DLS is not a suitable method to measure plateau-shaped nanomaterials; it was used to obtain the preliminary results. Moreover, it is shown that the zeta potential of the synthesised nanoplatform was as high as to provide acceptable dispersibility. SEM and TEM were obtained from the synthesised nanoplatform to observe the morphology and the real size (see Figs. 1 and 2). The SEM image (Fig. 1) illustrates the morphology of the synthesised nanocomplex in the agglomeration form, which is due to the sample preparation protocol. Moreover, GO sheets, as well as Fe and AuNPs, are present in this image.

TEM image was obtained to visualise the morphology of the synthesised nanocomplex. The image revealed that the nanocomplex has a typical two-dimensional sheet structure with the crumpled feature. Moreover, it is apparent from the TEM image that Fe and AuNPs are assembled onto the GO sheet and there are not any NPs outside the GO support even after strong sonication

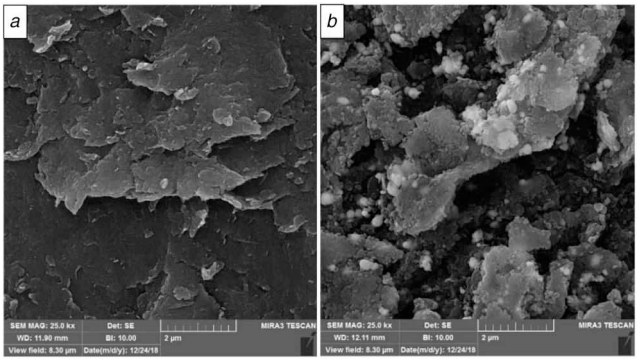


**Fig. 1** *SEM micrograph of*
***(a)*** GO, ***(b)*** Fe–AuNPs decorated GO

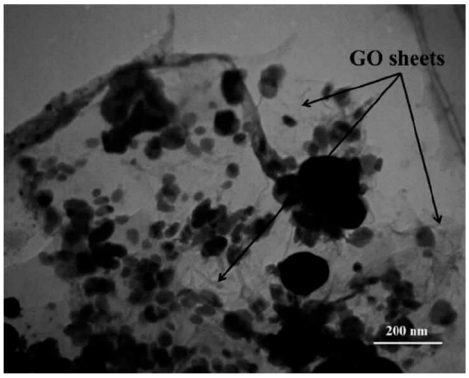


**Fig. 2** *TEM bright-field image obtained from the as-synthesised GO sheet*

used for TEM imaging. It is worth mentioning that the GO acted as the support to immobilise the NPs.

The combination of GO with metallic NPs has been subjected to the various studies conducted by other scientists. Kan and Wang synthesised $Fe_2O_3$–graphene nanocomposites and observed that graphene was able to support $Fe_2O_3$ assembly [34]. In another study, Goncalves *et al.* [35] utilised graphene sheets as the support for AuNPs formation. They reported that oxygen functional groups at the graphene surface act as the reactive sites for the nucleation and the subsequent growth of AuNPs. Huang *et al.* [36] decorated graphene with AuNPs through the non-covalent attachment using 2-mercaptopyridine. Although they did not use in situ NPs formation, GO effectively immobilised AuNPs as the supporting substrate. In another study, Chen *et al.* [32] fabricated multifunctional nanocomposites of $Fe_3O_4$–graphene–Au using in situ formation of AuNPs and $Fe_3O_4$ NPs on rGO. They reported that using the hydrothermal method, separate AuNPs and $Fe_3O_4$ NPs formed instead of Au/Fe alloy formation. Our results implied that the application of GO as the substrate material effectively support the in situ formation of Fe and AuNPs and prevent their agglomeration.

### *3.2 Fe–Au–GO nanocomplex toxicity results*

The MTT assay kit was used to assess the toxicity of the synthesised nanocomplex against MCF-7 cells, and the results are presented in Fig. 3. The results showed that up to near 50 ppm, there was no significant cell toxicity, while the higher concentration induced considerable toxicity, which was statistically significant against the control group ($P < 0.05$). The cell viability of the control, 10, 25, 50, 75, 100, 200 ppm groups were 100, 99, 93, 84, 74, 68, and 49%, respectively, after 24 h post-incubation. Accordingly, the 50 ppm concentration was chosen for the subsequent treatment studies. In a similar approach, Kumar *et al.* [37] synthesised FeNPs decorated GO as the RF hyperthermia agent for cancer treatment. They reported concentration-dependent cell toxicity and with the highest cell lethality at the concentration of 200 μg/ml.

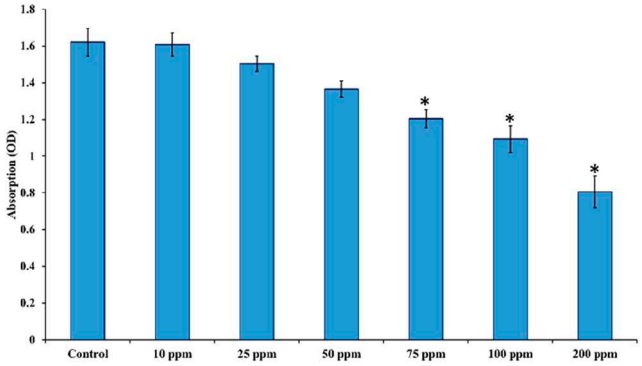


**Fig. 3** *Viability of MCF-7 cells under incubation of the prepared GO–Fe–AuNPs. The viability was measured by the MTT assay kit after 24 h post-incubation. N = 5, value = mean±SD, *P < 0.05*

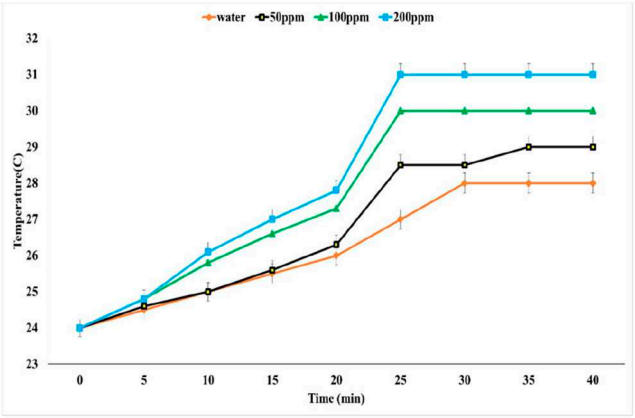


**Fig. 4** *Heating performance of the nanoplatforms under interaction with the RF field*

### *3.3 Thermal response of Fe–Au–GO nanocomplex under interaction with RF stimulation*

Thermal dissipation through the fabricated nanoplatforms under interaction with the 900 MHz RF field was assessed, and the results are presented in Fig. 4. As can be seen, the heating response was time and concentration-dependent, and the higher concentration of nanoplatforms resulted in higher temperature elevation.

The RF exposure conducted for 40 min, and it was observed that after 30 min, the temperature did not further increase, and the curve reached a plateau. Moreover, we predict that the final temperature of medium cells in incubator conditions will reach 41–42°C at RF field exposure. The exact underlying mechanism of the RF hyperthermia using NPs is not clearly proposed, although there are some possible mechanisms. In the case of AuNPs, three mechanisms have been proposed, including electrophoretic heating, magnetic heating, and Joule or inductive heating. The NP formulation, as well as parameters of the RF field character, determine, which mechanisms dominate heating [38]. On the other hand, in the case of magnetic NPs, susceptibility loss through Brownian rotation and Néel relaxation is proposed for heat generation [39].

### *3.4 Cell death-induced by Fe–Au–GO nanocomplex, RF and RT exposure*

According to the findings of toxicity and thermal profile assessment, the concentration of 50 ppm was chosen to apply the thermal effect on the cells. MCF-7 cells were seeded into the 96-well cell culture plate and divided into the control (without any treatments), NPs, RF, RT, NPs with RF, NPs + RT, and NPs with RF and RT (see Fig. 5).

The results showed that RF exposure without NPs did not induce significant toxicity, while RT exposure induced cell death, which was statistically significant in comparison with the control

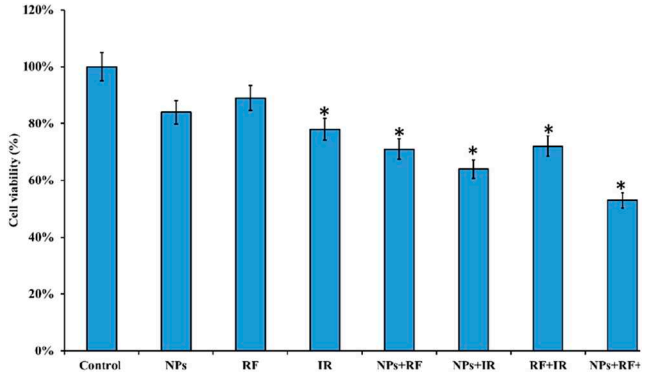


**Fig. 5** *Viability of MCF-7 cells under treatments with NPs and radiations. Cells were incubated with the nanoplatform and exposed to 900 MHz RF field for 30 min and 4 Gy RT. The cell viability was measured by the MTT assay kit. N = 5, value = mean±SD, *p < 0.05*

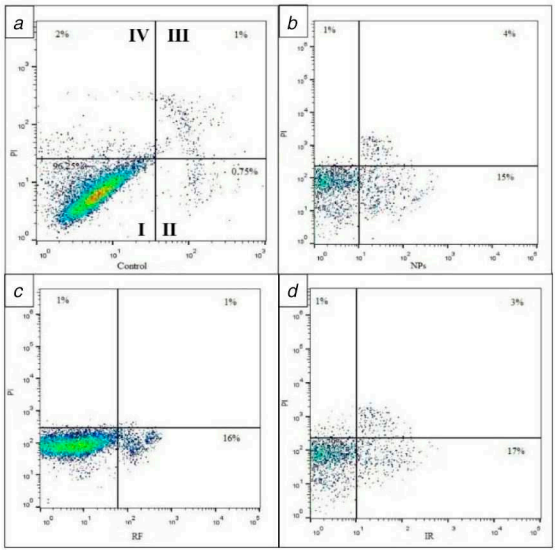


**Fig. 6** *Flow cytometric analysis of single therapy*
***(a)*** Control, ***(b)*** NPs, ***(c)*** RF, ***(d)*** RT. I: live cells; II: early apoptosis; III: late apoptosis; IV: necrosis

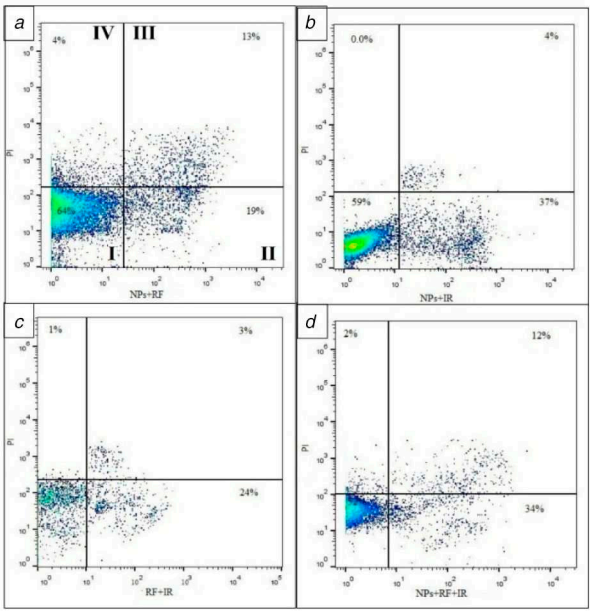


**Fig. 7** *Flow cytometric analysis of combination therapy*
***(a)*** NPs + RF, ***(b)*** NPs + RT, ***(c)*** RF + RT, ***(d)*** NPs + RF + RT. I: live cells; II: early apoptosis; III: late apoptosis; IV: necrosis

group ($P < 0.05$). The combination of NPs with RF exposure reduced the cell viability to around 71%, while NPs combination with RT resulted in 64% cell viability. These findings can be attributed to the ionising nature of RT exposure. Moreover, the highest cell dead was obtained with the combination of NPs with both RF and RT exposures with the cell viability of 53% ($P < 0.05$). These results confirmed the efficacy of the cancer cell treatment designed in the current study. Moreover, it is apparent that simultaneous exposure of cancer cells to RF and RT radiation provides the highest treatment efficacy.

### *3.5 Death-induced mechanism*

Flow cytometry assay was conducted to further evaluate the mechanism of cell growth suppression induced by the treatments. The results of flow cytometry assay are presented in Figs. 6 and 7. The results demonstrated that in the single therapies, 4Gy RT without NPs induced 20% apoptosis, while NPs without radiation and RF without NPs had no significant effects on cells.

The hybrid therapy revealed that the combination of NPs with radiation therapy induces significant cell toxicity through the apoptosis indication. The synergic effect of NPs with RF and RT radiations are presented in Figs. 7 and 8.

As shown in Figs. 7 and 8, the combination of NPs with radiations, RF, and RT, resulted in the highest treatment efficacy. Moreover, Fig. 8 presented that the early apoptosis was the main effect elicited with the treatment modalities.

Tumour hyperthermia has been the subject of various studies. Cardinal *et al.* conducted an in vitro and in vivo study to assess the hyperthermic effects of AuNPs under interaction with 13.56 MHz RF radiation. They reported that AuNPs did not induce any significant cytotoxic effects, while its combination with RF wave significantly induced lethal effects on HepG2 cells and reduced the tumour size. In another study, Gannon *et al.* utilised single-walled carbon nanotubes as the thermal dissipating agent under interaction with 13.56 MHz RF wave with the power of 800 W. They observed a dose-dependent temperature elevation and thermal-induced cell death. The in vitro and in vivo studies confirmed cancer cell eradicating effect of the proposed thermal therapy. Our findings also revealed dose-dependent temperature elevation, while we applied RF waves with a lower power (3 W).

In addition to the hyperthermia, the fabricated nanohybrid is a radiosensitising agent and enhanced the effects of RT. The combination of 50 ppm nanohybrid with RT induced 36% cell death. Our findings also indicated that the dose enhancement factor (DEF) of the nanohybrid was 1.63 and 2.63 for RT and RF, respectively. These results revealed that the heat-dissipating property of the prepared nanohybrid was prominent over its radiosensitising activity. Wolfe *et al.* [40] reported a DEF of 1.19 using PEGylated gold nanorods under radiation with 6 MV X-rays. They developed an effective treatment modality for breast cancer. In another study, Neshastehriz *et al.* [41] combined photothermal therapy and RT using folate-conjugated AuNPs against mouth epidermal carcinoma cells. They reported a DEF of 1.46 and high cancer cells eradication efficacy under the combination therapy in comparison with the single treatment models.

## 4 Conclusion

Nanostructures offer fascinating opportunities favourable for cancer diagnosis and treatment. Nanostructures exhibit size-dependent properties, which means that a single nanostructure has distinct properties in the same situation. Moreover, they have a high-surface area that provides sufficient surface to implement distinct treatment and diagnosis modalities simultaneously. In the current study, we utilised GO as the template and support for the synthesis of AuNP and iron NP (FeNP). The results confirmed that AuNP and FeNP were successfully synthesised on the GO surface. Heat measurement showed a dose- and time-dependent temperature elevation. The highest temperature obtained with 200 ppm concentration nanohybrid.

Moreover, the cell toxicity assay showed that the prepared nanohybrid did not induce significant cytotoxicity. Treatment results showed that single treatments using RF and RT exposure

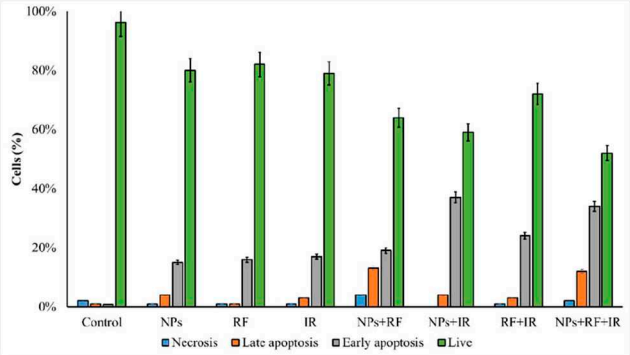


**Fig. 8** *Comparison of different modes of death and apoptosis rate in eight groups of single treated and combined treatments in MCF-7 cells*

slightly reduced the viability of the cells, while the combinatorial treatment significantly reduced the cell viability. Moreover, the DEF of 1.63 and 2.63 were obtained using the combination of the nanohybrid with RT and RF, respectively. These findings indicated that the prepared nanohybrid was a more heat-dissipating agent than a radiosensitising agent. In conclusion, this study demonstrated that GO could support AuNP and IONP, and the resulted nanohybrid can be considered as the combinatorial cancer treatment agent. For the future direction, the efficacy of the prepared nanohybrid as the contrast agent in MRI and X-ray computed tomography can be evaluated.

## 5 Acknowledgments

The authors gratefully acknowledge the research council of Kermanshah University of Medical Sciences (grant no. 980639) for financial support.

## 6 References

[1] DeSantis, C.E., Ma, J., Goding Sauer, A., *et al.*: 'Breast cancer statistics, 2017, racial disparity in mortality by state', *CA Cancer J. Clin.*, 2017, **67**, (6), pp. 439–448

[2] Mahmoodzadeh, F., Abbasian, M., Jaymand, M., *et al.*: 'A novel gold-based stimuli-responsive theranostic nanomedicine for chemo-photothermal therapy of solid tumors', *Mater. Sci. Eng. C*, 2018, **93**, pp. 880–889

[3] Poorgholy, N., Massoumi, B., Ghorbani, M., *et al.*: 'Intelligent anticancer drug delivery performances of two poly (*N*-isopropylacrylamide)-based magnetite nanohydrogels', *Drug Dev. Ind. Pharm.*, 2018, **44**, (8), pp. 1254–1261

[4] Falk, M., Issels, R.: 'Hyperthermia in oncology', *Int. J. Hyperth.*, 2001, **17**, (1), pp. 1–18

[5] Hahn, G.M.: '*Hyperthermia and cancer*' (Springer Science & Business Media, USA, 2012)

[6] Issels, R.D.: 'Hyperthermia adds to chemotherapy', *Eur. J. Cancer*, 2008, **44**, (17), pp. 2546–2554

[7] Kim, H.-C., Kim, E., Jeong, S.W., *et al.*: 'Magnetic nanoparticle-conjugated polymeric micelles for combined hyperthermia and chemotherapy', *Nanoscale*, 2015, **7**, (39), pp. 16470–16480

[8] Rodrigues, R.O., Baldi, G., Doumett, S., *et al.*: 'Multifunctional graphene-based magnetic nanocarriers for combined hyperthermia and dual stimuli-responsive drug delivery', *Mater. Sci. Eng. C*, 2018, **93**, pp. 206–217

[9] Fazal, S., Paul-Prasanth, B., Nair, S.V., *et al.*: 'Theranostic iron oxide/gold ion nanoprobes for MR imaging and noninvasive RF hyperthermia', *ACS Appl. Mater. Interfaces*, 2017, **9**, (34), pp. 28260–28272

[10] Kurgan, E., Gas, P.: 'Simulation of the electromagnetic field and temperature distribution in human tissue in RF hyperthermia', *Prz. Elektrotech.*, 2015, **91**, (1), pp. 169–172

[11] Nasseri, B., Kocum, I.C., Seymen, C.M., *et al.*: 'Penetration depth in nanoparticles incorporated radiofrequency hyperthermia into the tissue: comprehensive study with histology and pathology observations', *IET Nanobiotechnol.*, 2019, **13**, (6), pp. 634–639

[12] Esmaeili-Bandboni, A., Amini, S.M., Faridi-Majidi, R., *et al.*: 'Cross-linking gold nanoparticles aggregation method based on localised surface plasmon resonance for quantitative detection of MIR-155', *IET Nanobiotechnol.*, 2017, **12**, (4), pp. 453–458

[13] Amini, S.M., Kharrazi, S., Hadizadeh, M., *et al.*: 'Effect of gold nanoparticles on photodynamic efficiency of 5-aminolevolenic acid photosensitiser in epidermal carcinoma cell line: an in vitro study', *IET Nanobiotechnol.*, 2013, **7**, (4), pp. 151–156

[14] Mortezaee, K., Najafi, M., Samadian, H., *et al.*: 'Redox interactions and genotoxicity of metal-based nanoparticles: a comprehensive review', *Chemico-Biol. Interact.*, 2019, **312**, p. 108814

[15] Khoshnevisan, K., Daneshpour, M., Barkhi, M., *et al.*: 'The promising potentials of capped gold nanoparticles for drug delivery systems', *J. Drug Targeting*, 2018, **26**, (7), pp. 525–532

[16] Abbasian, M., Judi, M., Mahmoodzadeh, F., *et al.*: 'Synthesis and characterization of a pH- and glucose-responsive triblock copolymer via raft technique and its conjugation with gold nanoparticles for biomedical applications', *Polym. Adv. Technol.*, 2018, **29**, (12), pp. 3097–3105

[17] Chakaravarthi, G., Narasimhan, A.K., Rao, M.R., *et al.*: 'Influence of gold nanoparticles (GNPs) on radiofrequency tissue heating'. 2019 URSI Asia-Pacific Radio Science Conf. (AP-RASC), New Delhi, India, 2019

[18] Corr, S.J., Curley, S.A.: 'Gold nanoparticles for noninvasive radiofrequency cancer hyperthermia', in Mathur, A.B. (Ed.): *Nanotechnology in Cancer* (William Andrew Publishing, USA., 2017), pp. 1–18

[19] Naik, B., Dubey, S.K.: 'Gold coated cobalt nanoparticles as SAR controlling agent for hyperthermia applications'. 2017 IEEE MTT-S Int. Microwave and RF Conf. (IMaRC), Ahmedabad, India, 2017

[20] Pantano, P., Harrison, C.D., Poulose, J., *et al.*: 'Factors affecting the 13.56-MHz radio-frequency-mediated heating of gold nanoparticles', *Appl. Spectrosc. Rev.*, 2017, **52**, (9), pp. 821–836

[21] Dou, J.-P., Zhou, Q.-F., Liang, P., *et al.*: 'Advances in nanostructure-mediated hyperthermia in tumor therapies', *Curr. Drug Metab.*, 2018, **19**, (2), pp. 85–93

[22] Hemery, G., Garanger, E., Lecommandoux, S., *et al.*: 'Thermosensitive polymer-grafted iron oxide nanoparticles studied by in situ dynamic light backscattering under magnetic hyperthermia', *J. Phys. D, Appl. Phys.*, 2015, **48**, (49), p. 494001

[23] Gotman, I., Psakhie, S.G., Lozhkomoev, A.S., *et al.*: 'Iron oxide and gold nanoparticles in cancer therapy'. AIP Conf. Proc., Tomsk, Russia, 2016

[24] Abbasian, M., Razavi, L., Jaymand, M., *et al.*: 'Synthesis and characterization of poly(styrene-block-acrylic acid)/$Fe_3O_4$ magnetic nanocomposite using reversible addition-fragmentation chain transfer polymerization', *Sci. Iran.*, 2019, **26**, (3), pp. 1447–1456

[25] Amini, S.M., Akbari, A.: 'Metal nanoparticles synthesis through natural phenolic acids', *IET Nanobiotechnol.*, 2019, **13**, (8), pp. 771–777

[26] Mohammadi, M., Rezaei, A., Khazaei, A., *et al.*: 'Targeted development of sustainable green catalysts for oxidation of alcohols via tungstate-decorated multifunctional amphiphilic carbon quantum dots', *ACS Appl. Mater. Interfaces*, 2019, **11**, (36), pp. 33194–33206

[27] Adibi-Motlagh, B., Lotfi, A.S., Rezaei, A., *et al.*: 'Cell attachment evaluation of the immobilized bioactive peptide on a nanographene oxide composite', *Mater. Sci. Eng. C*, 2018, **82**, pp. 323–329

[28] Rezaei, A., Akhavan, O., Hashemi, E., *et al.*: 'Toward chemical perfection of graphene-based gene carrier via Ugi multicomponent assembly process', *Biomacromolecules*, 2016, **17**, (9), pp. 2963–2971

[29] Khalilzadeh, B., Shadjou, N., Afsharan, H., *et al.*: 'Reduced graphene oxide decorated with gold nanoparticle as signal amplification element on ultra-sensitive electrochemiluminescence determination of caspase-3 activity and apoptosis using peptide based biosensor', *Bioimpacts*, 2016, **6**, (3), p. 135

[30] Zaaba, N., Foo, K., Hashim, U., *et al.*: 'Synthesis of graphene oxide using modified hummers method: solvent influence', *Procedia Eng.*, 2017, **184**, pp. 469–477

[31] Ge, S., Shi, X., Sun, K., *et al.*: 'Facile hydrothermal synthesis of iron oxide nanoparticles with tunable magnetic properties', *J. Phys. Chem. C*, 2009, **113**, (31), pp. 13593–13599

[32] Chen, F., Wang, Y., Chen, Q., *et al.*: 'Multifunctional nanocomposites of $Fe_3O_4$–graphene–Au for repeated use in simultaneous adsorption, in situ SERS detection and catalytic reduction of 4-nitrophenol in water', *Mater. Res. Express*, 2014, **1**, (4), p. 045049

[33] Mortazavi, S., Erfani, N., Mozdarani, H., *et al.*: 'Induction of apoptosis by 900 MHz radiofrequency radiation emitted from a GSM mobile phone simulator in bystander Jurkat cells', *Int. J. Radiat. Res.*, 2015, **13**, (2), pp. 181–186

[34] Kan, J., Wang, Y.: 'Large and fast reversible Li-ion storages in $Fe_2O_3$-graphene sheet-on-sheet sandwich-like nanocomposites', *Sci. Rep.*, 2013, **3**, p. 3502

[35] Goncalves, G., Marques, P.A., Granadeiro, C.M., *et al.*: 'Surface modification of graphene nanosheets with gold nanoparticles: the role of oxygen moieties at graphene surface on gold nucleation and growth', *Chem. Mater.*, 2009, **21**, (20), pp. 4796–4802

[36] Huang, J., Zhang, L., Chen, B., *et al.*: 'Nanocomposites of size-controlled gold nanoparticles and graphene oxide: formation and applications in SERS and catalysis', *Nanoscale*, 2010, **2**, (12), pp. 2733–2738

[37] Kumar, R., Chauhan, A., Jha, S.K., *et al.*: 'Localized cancer treatment by radio-frequency hyperthermia using magnetic nanoparticles immobilized on graphene oxide: from novel synthesis to in vitro studies', *J. Mater. Chem. B*, 2018, **6**, (33), pp. 5385–5399

[38] Collins, C., McCoy, R., Ackerson, B., *et al.*: 'Radiofrequency heating pathways for gold nanoparticles', *Nanoscale*, 2014, **6**, (15), pp. 8459–8472

[39] Vallejo-Fernandez, G., Whear, O., Roca, A., *et al.*: 'Mechanisms of hyperthermia in magnetic nanoparticles', *J. Phys. D, Appl. Phys.*, 2013, **46**, (31), p. 312001

[40] Wolfe, T., Chatterjee, D., Lee, J., *et al.*: 'Targeted gold nanoparticles enhance sensitization of prostate tumors to megavoltage radiation therapy in vivo', *Nanomed. Nanotechnol. Biol. Med.*, 2015, **11**, (5), pp. 1277–1283

[41] Neshastehriz, A., Tabei, M., Maleki, S., *et al.*: 'Photothermal therapy using folate conjugated gold nanoparticles enhances the effects of 6 MV X-ray on mouth epidermal carcinoma cells', *J. Photochem. Photobiol. B, Biol.*, 2017, **172**, pp. 52–60